Atmos. Meas. Tech. Discuss., 8, 10577–10609, 2015
www.atmos-meas-tech-discuss.net/8/10577/2015/
doi:10.5194/amtd-8-10577-2015

Atmospheric Measurement Techniques Discussions

Relevance of a kite-based calibration for a water vapour Raman lidar

J. Totems and P. Chazette

Laboratoire des Sciences du Climat et de l'Environnement, CEA, Gif-sur-Yvette, France

Received: 6 August 2015 – Accepted: 29 September 2015 – Published: 15 October 2015

Correspondence to: J. Totems (julien.totems@cea.fr)

Published by Copernicus Publications on behalf of the European Geosciences Union.

Abstract

We present a calibration method for a water vapour Raman lidar using a meteorological probe on-board a kite, flown steadily above the lidar site, within the framework of the Hydrological Cycle in the Mediterranean Experiment (HyMeX) and Chemistry-Aerosols Radiative Effect in the Mediterranean (ChArMEx) campaigns. The experiment was carried on in Menorca (Spain) during June 2013, using the mobile Water vapour and Aerosol Lidar WALI. The kite calibration showed a much better degree of co-location with the lidar system than could be achieved with radiosondes, and allowed to calibrate measurements below the full overlap range between the emitter and the receiver. A range-dependent water vapour lidar calibration was determined, with an uncertainty of 2 % in the altitude range 90–8000 m. Water vapour measurements were further compared with radiosondes, showing very good agreement in the lower troposphere (1–5 km) and a relative mean and standard deviation of 5 and 9 %, respectively. Moreover, a reasonable agreement with MODIS integrated water vapour content is found, with a relative mean and standard deviation of 3 and 16 %. However, a discrepancy was found with AERONET retrievals, showing the latter to be underestimated by 28 %. Reanalyses from the ECMWF/IFS numerical weather prediction model were also in agreement with the temporal evolution highlighted with the lidar, with no measurable drift in integrated content over the period.

1 Introduction

The water vapour content is an essential parameter driving atmospheric dynamics in the boundary layer. Due to the hygroscopic properties of airborne particles (Randriamiarisoa et al., 2006), it also acts on the radiative balance at a global scale, one of the reasons why aerosols remain a major source of uncertainties in long term forecasts of radiative forcing on the climate (IPCC, 2014). For the past 3 years, within the French MISTRALS research program, the western Mediterranean basin has been the focus

AMTD
8, 10577–10609, 2015

of both water cycle (HyMeX, Drobinski et al., 2014) and aerosol radiative forcing studies (ChArMEx, Mallet et al., 2015) because of the important societal impact of climate change in this densely populated region, as well as its complex atmospheric circulation which makes both weather and chemical transport models fail at delivering reliable forecasts.

In this context, range-resolved profiles of aerosol extinction and water vapour mixing ratio (WVMR) obtained by lidar remote sensing are a powerful tool. Raman lidars can measure the latter parameter through the calibrated ratio of water vapour and nitrogen inelastic backscatter signals (Whiteman et al., 1992). During IHOP (Weckwerth et al., 2004) in the American great plains, a radiosonde-calibrated system (Whiteman et al., 2006a) allowed the first study of water vapour-driven convective processes in the boundary layer through the diurnal cycle (Whiteman et al., 2006b). The European study COPS (Wulfmeyer et al., 2011), performed in 2007 in the Rhine valley, showed among others that biases between several Raman and DIAL water vapour lidars and passive measurements remained below 5 % (Bhawar et al., 2011). Such systems still operational in Europe include Raman lidars BASIL (Di Girolamo and Summa, 2009) and IGN (Bock et al., 2013), the upper tropospheric/lower stratospheric Raman lidars at Haute-Provence (Sherlock et al., 1999a) and Réunion (Dionisi et al., 2015) observatories and the scanning DIAL of the University of Hohenheim (Behrendt et al., 2009).

The Water vapour and Aerosol LIdar WALI (Chazette et al., 2014a) is a portable and versatile system originally designed to meet the scientific goals of the first special observation period of HyMeX (the Hydrological Cycle in the Mediterranean Experiment, Ducrocq et al., 2014) in autumn 2012, dedicated to improving forecasts of extreme precipitation events on the orography of the western basin. It was also implemented as part of the Menorca Island (Spain) Cap d'en Font ground-based station during the June 2013 special observation period of the ADRIMed (Aerosol Direct Radiative Impact of the regional climate in the Mediterranean region, Mallet et al., 2015) segment of ChArMEx (the Chemistry-Aerosol Mediterranean Experiment), focused on the radiative impact of dust and anthropic aerosols.

AMTD
8, 10577–10609, 2015

The proper absolute calibration of the water vapour mixing ratio (WVMR) derived by a Raman lidar, with less than 0.4 $g\,kg^{-1}$ total uncertainty as demanded by meteorological and climate applications (Weckwerth et al., 1999), remains a critical issue. Indeed, it has been shown by several studies that a purely photometric calibration, on an laboratory optical bench, to determine the gain ratio of the H_2O and N_2 paths lacks precision and leads to significant bias on the retrieved WVMR (a few $g\,kg^{-1}$, $\sim 10\,\%$ in the lower troposphere) (Leblanc and McDermid, 2008; Whiteman et al., 2011). This calibration method also requires a common optical path before the field diaphragm of the lidar, which was dismissed for WALI in favour of modularity. A more precise yet practical approach using the sky background as a standard light source (Sherlock et al., 1999b) requires radiative transfer models and to eliminate all parasitic light sources. This was impossible in the setup of this field experiment, where an anti-dust blowing funnel was necessary above the lidar windows, which scattered some sunlight into the receptor. Raman lidars can also be calibrated using water vapour profiles given by a multi-channel microwave radiometer, as was done recently in the framework of the HD(CP)2 campaign in Germany, in an automated fashion (Foth et al., 2015). Yet this instrument is still unavailable commercially. In the end, co-located vertical sounding to deduce WVMR from temperature and RH measurements up to the stratosphere is the most precise method available, albeit limited by the accuracy of the meteorological probe. Radiosoundings are however rather heavy, with a costly apparatus and the request of a flight exclusion area to the air traffic control. Moreover, they may drift and not always be well co-located with the lidar. Whereas the spatial homogeneity of WVMR is generally good in the free troposphere, it is less so in the planetary boundary layer (PBL), especially in a coastal area or close to reliefs.

Incidentally, there is a long history of kite atmospheric sounding, which started with the "meteorographs" of Teisserenc de Bort at Trappes, France, in 1898. Despite an impressive altitude range (up to 9800 m in 1916), this technique somewhat tuned down during the 20th century in favour of weather balloons. It was rehabilitated and improved by the team of Balsley et al. (1992, 1998) at CIRES because of specific advantages.

AMTD
8, 10577–10609, 2015

Indeed, materials and fabrics evolved making kites lighter and inexpensive; they also offer the possibility of sounding the same layer for a longer time and remaining stationary, like tethered balloons. They have been applied to low altitude water-vapour sounding (Davidson et al., 2003) or used for aerosol profiling (Reiche et al., 2012). Willitsford and Philbrick (2005), used the data of Davidson et al. (2003) in synergy with a ground-based Raman lidar to describe the evapouration duct over the ocean. Generally, the use of kites is mainly constrained by wind conditions and locally strict regulations due to the ever-intensifying air traffic.

In this article, we present an original calibration process of a mobile water vapour Raman lidar using a kite-borne Vaisala pressure/temperature/RH probe, flying at low altitude where signal is strongest and biases due to temperature and aerosols transmission remain limited. This calibration is validated by comparisons to in-situ profiling, remote sensing of integrated water content, and outputs from a meteorological model.

In Sect. 2 we will describe the set-up of the kite payload and WALI lidar, along with the location of the experiment and the exogenous measurements used in this study. Section 3 will present the calibration process and the assessment of the associated uncertainties. The cross-validation is presented in Sect. 4, where the lidar-derived WVMR profile and integrated water vapour content (IWVC) are compared with radiosoundings, satellite measurements (MODIS), ground-based sunphotometer measurements and reanalyses by the numerical weather prediction model ECMWF/IFS (European Centre for Medium-range Weather Forecasts/integrated forecast system). Section 5 will summarize and conclude.

2 Experimental set-up

2.1 Location of the experiment

During the ADRIMed SOP-1 campaign in June–July 2013, a background station was deployed near the centre of the western Mediterranean, at Cap d'en Font (39°49′33″ N,

AMTD
8, 10577–10609, 2015

4°12′29″ E), a cape on the south coast of Menorca island (Fig. 1). This site was chosen to stay rather clear of local pollution sources in the dominant south-westerly winds. It offers the opportunity for sampling various air masses with contrasted water vapour amount within the lower and middle troposphere. Moreover, the windy south coast of Menorca island is a very suitable environment to use a light instrumented kite.

2.2 Raman lidar WALI

The WALI is a transportable lidar instrument mainly dedicated to atmospheric research activities (Chazette et al., 2014a, b). Emitting at 354.7 nm wavelength, it is designed to fulfil eye safety conditions. Its emitter is a pulsed Nd:YAG (Quantel Brilliant) laser. The UV pulse energy is ∼ 60 mJ and the pulse repetition frequency is 20 Hz. Its wide field-of-view of ∼ 2.3 mrad ensures a full-overlap of the transmission and reception paths beyond ∼ 200–300 m.

The system has four channels. On each channel, optical detection is performed by a photomultiplier tube (PMT) placed behind interferential filters (0.2 nm bandwidth) manufactured by Materion/Barr and a focusing lens. The amplification gain of the PMT between its anode and cathode is directly linked to the input high voltage (HV) chosen by the lidar acquisition software. Automatic HV variation allows optimizing the detection dynamic for both nighttime and daytime measurements (with strong sky background light). The acquisition system is based on a PXI technology with 12 bit digitizers running at 200 $MS\,s^{-1}$ (mega sampling per second), manufactured by National Instruments. During all the experiment acquisition was performed for mean profiles of 1000 laser shots leading to a temporal sampling close to 1 min.

The first channel is dedicated to the detection of the elastic molecular, aerosols and cloud backscatter from the atmosphere. The second and third boards are dedicated to the measurements of the inelastic nitrogen (N_2-channel, ∼ 387 nm) and water vapour (H_2O-channel, ∼ 407 nm) Raman backscattered signals, respectively. They are identical to the elastic channel except for interference filters centred at the respective wavelengths of the first Stokes vibrational lines for the two gases (386.65 ± 0.10 and

AMTD
8, 10577–10609, 2015

407.45 ± 0.15 nm filter bandpass respectively), and an extra dichroic beamsplitter on the H_2O channel for better rejection of the elastic returns (complete details are given in Chazette et al., 2014a).

The WVMR is obtained as the ratio between the signals recorded by the N_2O- and N_2-Raman channels. In previous experiments with a properly calibrated WALI (Chazette et al., 2014a), the uncertainty on the WVMR reached 11 % in the marine boundary layer (MBL) and decreased to 7 % below 5 km range, with temporal averaging over 20 min and a nominal vertical resolution of 15 m. Precision deteriorated quickly above 5 km a.m.s.l. due to the decreasing signal, which we compensate here with larger averaging. The determination of the water vapour profile is more difficult during daytime, but the measurements have been performed with sufficient precision for altitude ranges below ∼ 1 km a.m.s.l. using temporal averaging over ∼ 30 min. A low-altitude WVMR calibration directly above the lidar is especially interesting considering that the progressive overlap of the lidar emission and reception paths biases WVMR up to 300 m, as noticed in the previous deployment of the lidar.

2.3 Water vapour sounding

Radiosondes were launched on weather balloons, along with particle and ozone counters, by a team from CNES led by N. Verdier, at the Sant-Lluis air field (39°51′56″ N, 4°15′17″ E), located 8 km northeast of the WALI lidar at Cap d'en Font. Only on this airfield could radiosounding be organized, authorized and made compatible with air traffic to and from the nearby Mahon airport, whereas the aerosol/lidar station needed to stay on the coast.

The characteristics of the Modem M10 GPSondes used are given in Table 1. From this data, an absolute uncertainty of 1.2 g kg^{-1} is expected near the ground (mostly due to the inaccuracy of the GPS altitude), which goes down to 0.04 g kg^{-1} at 10 km a.m.s.l.

In contrast, kites could be launched directly from Cap d'en Font, 100 m away from the lidar. The apparatus used for kite sounding is shown on Fig. 2. The kites were both "rokkaku" hexagonal kites (1.3 or 1.5 m width, for winds 3–15 m s^{-1}, known for

AMTD
8, 10577–10609, 2015

their stability) at the end of a single 650 m nylon line, carrying a lightweight (360 g) probe and datalogger (Vaisala PTB-110 barometer + Vaisala SP 2000-35R T/RH/V datalogger + 2 × 9 V batteries). Data was recorded every 10 s and retrieved after the flight. Given the specifications recalled in Table 1, the expected absolute accuracy on each WVMR sample is 0.6 g kg^{-1}.

2.4 Spaceborne measurements and numerical weather prediction model

On board the Aqua and Terra satellite, launched in the early 2000's as part of the Earth Observing System, the Moderate-resolution Imaging Spectroradiometer (MODIS) captures images in 36 spectral bands to provide measurements of large-scale global dynamics, including in the lower atmosphere. MODIS level 3 datasets are available online from NASA (https://earthdata.nasa.gov/labs/worldview/). They include daily precipitable water vapour data that are given on a 1° grid on both land and sea, with sufficient accuracy to allow comparison with ground-based measurements of water vapour (Gao and Kaufman, 2003).

Modelled synoptic-scale meteorological fields (geopotential height, temperature, moisture) have been obtained, over a large domain around the western Mediterranean, from the Integrated Forecast System (IFS) of the European Centre for Medium-range Weather Forecasts (ECMWF, http://www.ecmwf.int). The 3-D fields, available at the ESPRI/IPSL data server, are 6 hourly reanalyses with a horizontal resolution of 0.5°. The ECMWF model produces a good representation of the low-resolution moisture field as demonstrated in previous works (Chazette et al., 2014b).

3 Lidar calibration

With the WALI lidar, the WVMR profile is obtained as:

$$r_{\mathrm{H_2O,lidar}}(z) = K_{\mathrm{WVMR}} \frac{S_{\mathrm{H_2O}}(z)/\xi_{\mathrm{H_2O}}(z)}{S_{\mathrm{N_2}}(z)/\xi_{\mathrm{N_2}}(z)} \exp(\Delta\tau(z)), \quad (1)$$

AMTD
8, 10577–10609, 2015

where K_{WVMR} is a constant to be calibrated, $S_{H_2O}(z)$ and $S_{N_2}(z)$ are the lidar signals in the indexed channels, expressed as a function of altitude z, $\xi_{H_2O}(z)$ and $\xi_{N_2}(z)$ are the lidar overlap factors of the indexed channels (both reach 1 above 400 m), and $\Delta\tau(z)$ is the difference of total optical thickness between wavelengths 387 and 407 nm, which has to be estimated from the aerosol channel and corrected (thus avoiding a bias of up to 10 % above 4 km a.m.s.l., as estimated from our uncorrected signals). We do not consider temperature dependence of the Raman lines, as the H_2O-Raman interference filter is chosen at an insensitive wavelength following Whiteman et al. (2006a). The reception channels of the lidar were left confined and untouched during the entire course of the campaign to limit variations of the calibration parameters such as was reported by Bock et al. (2014). We trust that this protocol allowed the complete stability found between two calibrations of the WALI, 3 months apart, in its previous involvement (Chazette et al., 2014a).

The overlap function $\xi_{N_2}(z)$ of the N_2-Raman channel is estimated in a homogeneous atmosphere, as provided by a profile with the lidar set up horizontally. In order to assess the missing K_{WVMR} and $\xi_{H_2O}(z)$ in Eq. (1), we perform simultaneous measurements of water vapour by kite ($r_{H_2O,kite}(z)$) and lidar, and compute the following calibration function:

$$C(z) = \frac{S_{H_2O}(z)}{S_{N_2}(z)/\xi_{N_2}(z)} \frac{1}{r_{H_2O,kite}(z)} = \frac{1}{K_{WVMR}} \xi_{H_2O}(z), \quad (2)$$

the shape of which will be that of overlap factor $\xi_{H_2O}(z)$, and the value at high altitude will yield calibration coefficient K_{WVMR}.

Three flights were performed to assess calibration function $C(z)$. An important practical constraint was that they had to be done in daylight conditions, under which the lidar profiles are affected by sky background noise. Indeed, kite flight is more risky and often restricted in the absence of light. After an initial flight on 22 June afternoon up to 140 m, it was determined that the full overlap zone had not been reached. A following flight on 25 June morning, up to 390 m, passed the required altitude to estimate the calibration

AMTD
8, 10577–10609, 2015

coefficient. Finally, a third flight was performed on 25 June right during sunset when sky background light was low, to better assess the lowest values of the overlap function, from 0 to 115 m. Note that while this represents the best conditions for lidar calibration, care should be taken about the quick fall of wind strength that frequently occurs at dusk (as experienced on 23 and 24 June) and the kite launched slightly beforehand.

The computed $C(z)$ are given in Fig. 3. The resulting assessment of K_{WVMR} is $94.8 \pm 2.0\,g\,kg^{-1}$, as a mean over the 3 flights. The uncertainty, estimated between 0.4 and $1.7\,g\,kg^{-1}$ for each individual flight assuming randomly distributed error with altitude, is predominantly due to lidar noise above 100 m during daytime, and to sounding errors at lower altitude or at dusk. Residual standard deviation on the final result will be due to fluctuating bias on either one of the instrument. 50 % overlap is obtained at ~ 90 m; in the following WVMR retrievals, we correct the overlap function down to that altitude and discard the lower profile. We note an unusual shape of the overlap function with a plateau around 50–70 m. Rather than pointing towards a wrong estimation of the N_2 overlap function, verified on 5 separate occurrences, this effect has already been seen on the elastic channel of other lidars with the same design, and has been associated to a bad re-collimation of the received beam on the spectral filtering components. The response of the dichroic beamsplitter and interference filter (see Chazette et al., 2014a) to close object points with even more inclined rays is very variable and may explain this effect. Better focusing of the system on an optical bench should attenuate this phenomenon in future implementations.

4 Validation

In order to validate the kite-calibrated WVMR profile provided by WALI, we first compare it to the radiosoundings performed at Sant Lluis airfield during the beginning of the ADRIMed campaign (12–17 June 2013), a period characterized by several pollution transport events, followed by a Saharan dust event. We then study the correlation of lidar WVMR profiles with farther but more frequent radiosoundings, performed twice

AMTD
8, 10577–10609, 2015

daily at Palma de Majorca. Finally, we compare the integrated profile in terms of precipitable water vapour to the retrievals of the AERONET sunphotometer, the Aqua/MODIS instrument and the ECMWF reanalyses, to study the stability the calibration factor.

4.1 Comparisons to local rawinsoundings

Figure 4 shows the comparison of lidar-derived WVMR to the measurements of balloon radiosondes during their ascent. Note that the lidar integration time is equal to the duration of the ascent phase, approximately 40 min. We recall that the radiosonde uncertainty (not shown for better clarity) is $\sim 1.2\,\mathrm{g\,kg^{-1}}$ at ground level, down to $0.04\,\mathrm{g\,kg^{-1}}$ at 10 km a.m.s.l.; the lidar WVMR uncertainty, calculated as in Chazette et al. (2014a), is shown in blue. For reference, potential temperature, wind sector and velocity given by the sonde and the backscatter coefficient profile given by the lidar are shown. Origins and contents of air masses as deduced by backtrajectories (HYSPLIT, Draxler and Rolph, 2015) and optical parameters (lidar ratio, particle depolarization ratio) are given in plain text.

Overall very good agreement is observed in all the comparisons, except at sharp transitions. The altitude of transitions is sometimes shifted and absolute values of WVMR can differ in thin layers. The largest discrepancies occur near the ground, making these non-colocated radiosoundings unsuitable for the measurement of the overlap factor. Moreover, strong deviations are seen in a dust layer on the evening of 16 June; this effect remains unexplained, as the most important inhomogeneity, corresponding to a change in circulation, occurred 24 h earlier with little effect.

We assess the calibration factor K_{WVMR} that would have been obtained by using the ratio between radiosounding and lidar, averaged between 1 and 6 km a.m.s.l. and over all profiles: $K_{\mathrm{WVMR}} = 95.7 \pm 3.5\,\mathrm{g\,kg^{-1}}$. This is compatible to the result of calibration by kite: no drift of the calibration factor is measured during the span of 13 days covered by these comparisons. Note that the above standard deviation, computed using the lidar profile error and the specifications of Table 2, shows a higher value than with the kite, which seems due to the horizontal inhomogeneity of WVMR and maybe also

AMTD
8, 10577–10609, 2015

to the shorter averaging time available with balloons quickly ascending through the troposphere.

After the measurements of Fig. 4, the mean absolute difference between lidar-derived WVMR vs. that of balloon radiosondes is under $\pm 0.2\,g\,kg^{-1}$ across the whole profile. Absolute SDs are $\sim 1\,g\,kg^{-1}$ (RMS) below 1 km a.m.s.l., $< 0.6\,g\,kg^{-1}$ above 1 km a.m.s.l., and $< 0.2\,g\,kg^{-1}$ above 7 km a.m.s.l. The mean relative difference (i.e. 200 % (Lidar – Sonde)/(Lidar + Sonde)) is under ±5 % until 7 km a.m.s.l. Relative SD reaches 13 % (RMS) near the ground, is under 8 % between 1 and 4 km a.m.s.l., and grows to 12 % at 7 km a.m.s.l. At higher altitudes, it diverges up to 40 % at 10 km a.m.s.l.; indeed depending on signal-to-noise ratio the maximum range of the lidar can be reached between 7.5 and 10 km a.m.s.l., above which the retrieved WVMR is null per our processing algorithm.

Note that the balloons have already travelled between 15 and 20 km away from the lidar when at 7 km a.m.s.l. Recently, the fine scale horizontal structure function of WVMR in the free troposphere was assessed using a DIAL lidar on board a plane travelling across several hundreds of kilometers (Fischer et al., 2013). By taking, from Fig. 2 of the given reference, the order 2 structure function estimated at 4.1 km a.m.s.l. in a non-convective case, one can straightforwardly estimate the root mean square difference of WVMR between two points horizontally separated by distance d to scale as: $\Delta r_{H_2O,RMS}(d)/\langle r_{H_2O}\rangle \approx 14\,\% \,(d/10\,km)^{0.6}$. This amounts to $\sim 19\,\%$ for the balloon drift of 20 km given above, and would explain a majority of the observed RMS difference between lidar and balloons around this altitude.

4.2 Long-term correlation with operational radiosoundings and NWP model

In order to extend this validation to a broader dataset, we use the operational meteorology radiosoundings performed twice daily at Palma de Majorca (39°34′ N, 2°39′ E, 135 km ESE of Cap d'en Font), and compare it to a longer period of lidar measurements (12–28 June) in Fig. 5a and b).

AMTD
8, 10577–10609, 2015

In the following, we use root mean square error ($\mathrm{RMSE}(x,y) = \langle (x-y)^2 \rangle$), and correlation ($\mathrm{COR}(x,y) = \langle (x-\langle x \rangle)(y-\langle y \rangle) \rangle / (\mathrm{var}(x)\mathrm{var}(y))^{1/2}$) between two measurements as defined in (Boylan and Russell, 2006). They are plotted as bars in Fig. 5c and d. Also plotted as lines are the same variables computed between ECMWF/IFS profiles over Palma and Cap d'en Font, giving an idea of the natural variability along the baseline. The excess RMSE and lower COR will be due to the true lidar & radiosounding errors, independently from their separation.

Whereas several structures and dry layers can visibly be found in both measurements (sometimes shifted in time), it is noticeable that moisture levels are rather different in the lower layers (below 3 km a.m.s.l.). In the second part of the period especially (after 23 June), when winds turn N/NW (perpendicular to the baseline joining the two stations), WVMR is $\sim 20\,\%$ higher close to the ground in Majorca. Indeed, while over 4 km a.m.s.l. RMSE remains under $1\,\mathrm{g\,kg^{-1}}$, it reaches $2.5\,\mathrm{g\,kg^{-1}}$ under 3 km a.m.s.l. (half of which is due to the natural variability). Similarly, correlation (which is less dependent on the WVMR value) is around 0.67 between 2 and 6 km a.m.s.l., but falls to 0.2 below and above. Stronger decorrelation around 1.5 km a.m.s.l. (resp. above 7 km a.m.s.l.) seems mostly due to the lidar measurement noise during daytime (resp. night-time). The moderate value of correlation (~ 0.6–0.7) in the middle free troposphere is also partly due to the long baseline between the lidar and Palma (135 km). There is however a gap of about 0.2 between the theoretical and the measured correlations, attributable either to the lidar or to the radiosondes.

We also directly compare the lidar WVMR profile measurements to the ECMWF/IFS reanalyses over Menorca, resulting in the scatter plot shown in Fig. 6a). It demonstrates very little bias in terms of lidar calibration, except for the lower values ($< 2\,\mathrm{g\,kg^{-1}}$) which are mostly found in the upper layers that can be out of range of the lidar. There is however some dispersion around the identity line, investigated against altitude in terms of RMSE and COR in Fig. 6b and c. We see that the higher RMSE ($\sim 1.5\,\mathrm{g\,kg^{-1}}$) between lidar and model occur mostly in the lower troposphere (below 3 km), where moisture

AMTD
8, 10577–10609, 2015

may vary rapidly and might not be well resolved by the model. Above 3 km a.m.s.l., correlation around 0.9 is found.

In conclusion, we see in both comparisons the impact of a strong WVMR inhomogeneity in the lower layers including the marine boundary layer (< 500 m a.m.s.l.). In the free troposphere, WVMR profiles by lidar are well correlated with other measurements and model-derived moisture data, further validating WALI and its calibration over a long period.

4.3 Inter-comparisons of integrated water content

Thanks to the ability of the calibrated lidar to measure the bottommost layers (down to 90 m), another quantitative comparison can be made by integrating the night-time WVMR lidar profile over the whole atmospheric column to obtain precipitable water vapour content (PWV) WV_p as

$$WV_p = \int_{z=0}^{z=z_{max}} \frac{\rho_{air,dry}(z)}{\rho_{water}} r_{H_2O}(z) dz \quad (3)$$

with z_{max} the maximum altitude of the night-time lidar measurements (z_{max} = 10 km a.m.s.l.), $\rho_{air,dry}(z)$ the density profile of dry air, which is here deduced from the ECMWF model, and $\rho_{water} = 10^3$ kg m^{-3} the density of water. Note that the lidar WVMR profiles have been prolonged down to the ground, by linearly interpolating between the value at 90 m a.g.l. and the measurement of a Vaisala PTU-1000 on a 6 m a.g.l. mast at the ground-based station.

Lidar PWV can be compared directly to that derived from the WVMR profiles obtained by radiosounding at Sant Lluis and by the ECMWF model, but also to products given by MODIS on Terra & Aqua (discarding cloudy pixels with lower PWV). The aim of this section is not to inter-compare water vapour measurement techniques, which has been done extensively elsewhere (e.g. Bock et al., 2013), but to further validate

AMTD
8, 10577–10609, 2015

the accuracy of the lidar and especially the stability of the calibration factor, shown to vary by 17 % over 45 days in the same study.

PWV retrievals are plotted as a function of time for the 12–29 June period in Fig. 7. The AERONET sunphotometer-derived PWV and the MODIS PWV level 2 product show the most discrepancies with other measurements.

The sunphotometer PWV did not pass 3 cm for the whole period, generating a strong mean negative bias of −0.93 cm compared to the lidar. The strong diurnal variation on sunphotometer-derived PWV observed in the figure seems to be correlated with the diurnal evolution of the solar zenith angle. While several studies have commended the reliability of the AERONET retrieval, compared to GPS for instance (Bock et al., 2013), others warn about a slight dry bias (Pérez-Ramirez et al., 2014), the impact of misty and slightly cloudy weather (Liu et al., 2013) or of an improper calibration of the sunphotometer (Schmid et al., 2001). Yet, the lidar observations ensure that sunphotometer measurements were acquired under perfectly cloud-free conditions, the sunphotometer was recently calibrated, and the AERONET retrieval at Palma (not shown here) is similarly very strongly biased. This excludes both weather- or instrument-related problems, and points towards a systematic error of the retrieval method or calibration process.

For MODIS, the PWV uncertainty is estimated to lie between 5 and 10 % (Gao and Kaufman, 2003), which explains part of the discrepancies observed (about 15 % SD overall). On 12, 22, and 29 June however, the MODIS retrieval is significantly lower than that of the lidar. A possible explanation is that on these days, cirrus contamination is suspected over the whole area, which would have biased MODIS PWV (given “above the cloud level”) towards lower values.

In contrast, both ECMWF and radiosonde retrievals lie much closer to the lidar values (5.5 and 4.5 % RMSE respectively), validating the soundness of absolute lidar-derived PWV. The largest difference is seen on 14 June, when a very dry layer is seen extending down to 2 km a.m.s.l. by the lidar, whereas the ECMWF/IFS model does not see it as low. This can explain the larger PWV found by the model. Excluding this particular data, the relative mean (resp. standard) deviation between lidar and other retrievals is

AMTD
8, 10577–10609, 2015

only −1 % (resp. 11 % RMSE). If we further restrain the comparison to the most reliable data given by radiosoundings and ECMWF/IFS, SD is less than 6 %. No consistent drift is found, above these random errors, for the calibration factor of the lidar, over the 17 days of this study, in contrast to other instruments. If there is a drift, it must be much smaller than 10 %. This good stability may be due to the careful confinement of the lidar in the MAS van, equipped with powerful air conditioning.

5 Summary and conclusions

The aerosol/H_2O/N_2-Raman lidar WALI was implemented in response to the main scientific questions of the HyMeX program about the water cycle over the western Mediterranean basin. In the framework of the ChArMEx/ADRIMED special observation period, WALI was deployed on Menorca Island in June–July 2013 for complementary studies on tropospheric water vapour content and aerosols. During each field experiment, the WVMR profiles derived from WALI measurements have to be calibrated locally for maximum accuracy and to retrieve the overlap factor of the lidar. Radiosoundings measurements may be not relevant because of air mass motion or balloon drifting, and thus a lack of spatiotemporal coherence with the lidar. In our case, due to the separation between the launch site and the lidar station, the RMSE could reach $\sim 1\,g\,kg^{-1}$ in the first kilometres of the troposphere.

We used a meteorological probe on-board a kite launched from the lidar site, allowing a relative uncertainty of 2 % on WVMR calibration, down to 90 m a.g.l., thanks to the co-located measurement and the slower ascent permitted by the kite. After several trials, a ∼ 45 min flight up to 300 m at dusk (for better lidar signal-to-noise ratio) seems to be optimal for this method. The calibration uncertainty achieved with this method is better than the one reached for the previous deployment of WALI with radiosoundings and a plane-carried sonde (Chazette et al., 2014a). It is predominantly due to lidar noise above 200 m during daytime, and to sounding errors at lower altitude or at dusk. This relative uncertainty value is in the same range as that obtained

AMTD
8, 10577–10609, 2015

with microwave radiometers over long periods (1.4 %, Foth et al., 2015) and better than what is reached with several night-time radiosoundings (4.5 %, Whiteman et al., 2006a, confirmed here). We find that the kite-borne method has suitable precision while being lighter to implement.

The calibrated WVMR profiles have been cross-compared with radiosoundings, as well as integrated moisture derived from satellite measurements and the ECMWF/IFS reanalyses. The profiles are shown to be in very good agreement in the free troposphere (1–5 km a.m.s.l., mean deviations within 0.2 g kg^{-1} absolute, ±5 % relative), less so in the marine planetary boundary layer due to inhomogeneity, and above 7–8 km a.m.s.l. due to the range limitation of the lidar. Deviations between integrated water vapour contents appear to be within 6 % RMSE (compared to model reanalyses and local radiosoundings), and no drift is reported over the measurement period of ∼ 3 weeks. The MODIS level-2 data of PVW are in better agreement with a RMSE ∼ 15 % comparatively with the PWV derived from WALI. Larger discrepancies (more than −1 cm bias) are however observed when considering the sunphotometer-derived PWV. The fact that sunphotometer measurements were acquired in verifiably cloud-free conditions, that the sunphotometer was recently calibrated, and that the AERONET retrievals at Palma are similarly very strongly biased, excludes both weather- or instrument-related problems, and points towards a systematic error of the retrieval method or calibration process. It may still be specific to the conditions experienced in the Balearic sea during this period. While one previous study has warned about a slight dry bias (Pérez-Ramirez et al., 2014), this much stronger effect has not been reported elsewhere, to our knowledge. It should be investigated further, by comparison to GPS networks retrievals for instance, in similar conditions. Yet overall, the lidar calibration is found accurate and stable over the period.

Assuming full lidar overlap at the maximum sounding altitude and no bias at higher altitude, kite sounding thus appears as a practical and reliable way to calibrate both the water vapour retrieval and the overlap factor of a H_2O-Raman lidar, thanks to maximum signal-to-noise ratio, longer sounding and immediate proximity to the lidar beam.

AMTD
8, 10577–10609, 2015

Limitations include the need for good wind conditions, although only a couple knots are enough and frequent in many open sites, and regulations due to air traffic control, which vary geographically. This technique may be extended to any physical parameter measurable both by a lidar and a probe weighting less than a kilogram, such as temperature, aerosol size distribution, concentration or optical properties.

Acknowledgement. The authors thank P. Fabre for providing the kites, as well as S. Hassanzadeh, S. Bertolin, and M. Jeannot for their precious help during the kite sounding. The lidar station at Menorca was set-up and maintained with the help of F. Dulac, F. Marnas, X. Shang from LSCE, and M. Sicard, C. Munoz, and D. Lange from Universitat de Catanlunya. Balloon radiosoundings were performed by N. Verdier from CNES. This work was funded by the HyMeX and ChArMEx components of the MISTRALS program and by the Commissariat à l'Energie Atomique.

References

Behrendt, A., Wulfmeyer, V., Riede, A., Wagner, G., Pal, S., Bauer, H., Radlach, M., and Späth, F.: 3-Dimensional observations of atmospheric humidity with a scanning differential absorption lidar, in: Proc. SPIE Vol. 7475, Remote Sensing of Clouds and the Atmosphere XIV, edited by R. H. Picard, K. Schäfer, A. Comeron, and M. van Weele, 74750L, doi:10.1117/12.835143, 2009.

Bhawar, R., Di Girolamo, P., Summa, D., Flamant, C., Althausen, D., Behrendt, A., Kiemle, C., Bosser, P., Cacciani, M., Champollion, C., Di Iorio, T., Engelmann, R., Herold, C., Müller, D., Pal, S., Wirth, M., and Wulfmeyer, V.: The water vapour intercomparison effort in the framework of the convective and orographically-induced precipitation study: airborne-to-ground-based and airborne-to-airborne lidar systems, Q. J. Roy. Meteor. Soc., 137, 325–348, doi:10.1002/qj.697, 2011.

Bock, O., Bosser, P., Bourcy, T., David, L., Goutail, F., Hoareau, C., Keckhut, P., Legain, D., Pazmino, A., Pelon, J., Pipis, K., Poujol, G., Sarkissian, A., Thom, C., Tournois, G., and Tzanos, D.: Accuracy assessment of water vapour measurements from in situ and remote sensing techniques during the DEMEVAP 2011 campaign at OHP, Atmos. Meas. Tech., 6, 2777–2802, doi:10.5194/amt-6-2777-2013, 2013.

AMTD
8, 10577–10609, 2015

Boylan, J. W. and Russell, A. G.: PM and light extinction model performance metrics, goals, and criteria for three-dimensional air quality models, Atmos. Environ., 40, 4946–4959, doi:10.1016/j.atmosenv.2005.09.087, 2006.

Chazette, P., Marnas, F., and Totems, J.: The mobile Water vapor Aerosol Raman LIdar and its implication in the framework of the HyMeX and ChArMEx programs: application to a dust transport process, Atmos. Meas. Tech., 7, 1629–1647, doi:10.5194/amt-7-1629-2014, 2014a.

Chazette, P., Marnas, F., Totems, J., and Shang, X.: Comparison of IASI water vapor retrieval with H_2O-Raman lidar in the framework of the Mediterranean HyMeX and ChArMEx programs, Atmos. Chem. Phys., 14, 9583–9596, doi:10.5194/acp-14-9583-2014, 2014b.

Davidson, K. L., Guest, P. S., Mabey, D. L., Frederickson, P. A., Anderson, K. D., Doss-Hammel, S. M., and Tsintikidis, D.: The use of kite observations to study air–sea interaction-controlled atmospheric surface layer profiles during the RED experiment, in: 12th Conference on Interactions of the Sea and Atmosphere, vol. 1, 2003, available at: http://calhoun.nps.edu/public/handle/10945/41312, last access: 19 September 2014.

Di Girolamo, P., Summa, D., Lin, R.-F., Maestri, T., Rizzi, R., and Masiello, G.: UV Raman lidar measurements of relative humidity for the characterization of cirrus cloud microphysical properties, Atmos. Chem. Phys., 9, 8799–8811, doi:10.5194/acp-9-8799-2009, 2009.

Dionisi, D., Keckhut, P., Courcoux, Y., Hauchecorne, A., Porteneuve, J., Baray, J. L., Leclair de Bellevue, J., Vérèmes, H., Gabarrot, F., Payen, G., Decoupes, R., and Cammas, J. P.: Water vapor observations up to the lower stratosphere through the Raman lidar during the Maïdo Lidar Calibration Campaign, Atmos. Meas. Tech., 8, 1425–1445, doi:10.5194/amt-8-1425-2015, 2015.

Draxler, R. R. and Rolph, G. D.: HYSPLIT (HYbrid Single-Particle Lagrangian Integrated Trajectory) Model access via NOAA ARL READY Website, NOAA Air Resour. Lab. Silver Spring, MD, available at: http://ready.arl.noaa.gov/HYSPLIT.php, last access: 20 August, 2015.

Drobinski, P., Ducrocq, V., Alpert, P., Anagnostou, E., Béranger, K., Borga, M., Braud, I., Chanzy, A., Davolio, S., Delrieu, G., Estournel, C., Boubrahmi, N. F., Font, J., Grubišić, V., Gualdi, S., Homar, V., Ivančan-Picek, B., Kottmeier, C., Kotroni, V., Lagouvardos, K., Lionello, P., Llasat, M. C., Ludwig, W., Lutoff, C., Mariotti, A., Richard, E., Romero, R., Rotunno, R., Roussot, O., Ruin, I., Somot, S., Taupier-Letage, I., Tintore, J., Uijlenhoet, R., and Wernli, H.: HyMeX: A 10-year multidisciplinary program on the mediterranean water cycle, B. Am. Meteorol. Soc., 95, 1063–1082, doi:10.1175/BAMS-D-12-00242.1, 2014.

AMTD
8, 10577–10609, 2015

Ducrocq, V., Braud, I., Davolio, S., Ferretti, R., Flamant, C., Jansa, A., Kalthoff, N., Richard, E., Taupier-Letage, I., Ayral, P.-A., Belamari, S., Berne, A., Borga, M., Boudevillain, B., Bock, O., Boichard, J.-L., Bouin, M.-N., Bousquet, O., Bouvier, C., Chiggiato, J., Cimini, D., Corsmeier, U., Coppola, L., Cocquerez, P., Defer, E., Delanoë, J., Di Girolamo, P., Doerenbecher, A., Drobinski, P., Dufournet, Y., Fourrié, N., Gourley, J. J., Labatut, L., Lambert, D., Le Coz, J., Marzano, F. S., Molinié, G., Montani, A., Nord, G., Nuret, M., Ramage, K., Risøn, W., Roussot, O., Said, F., Schwarzenboeck, A., Testor, P., Van Baelen, J., Vincendon, B., Aran, M., and Tamayo, J.: HyMeX-SOP1: the field campaign dedicated to heavy precipitation and flash flooding in the northwestern Mediterranean, B. Am. Meteorol. Soc., 95, 1083–1100, doi:10.1175/BAMS-D-12-00244.1, 2014.

Fischer, L., Craig, G. C., and Kiemle, C.: Horizontal structure function and vertical correlation analysis of mesoscale water vapour variability observed by airborne lidar, J. Geophys. Res. Atmos., 118, 7579–7590, doi:10.1002/jgrd.50588, 2013.

Foth, A., Baars, H., Di Girolamo, P., and Pospichal, B.: Water vapour profiles from Raman lidar automatically calibrated by microwave radiometer data during HOPE, Atmos. Chem. Phys., 15, 7753–7763, doi:10.5194/acp-15-7753-2015, 2015.

Gao, B.-C. and Kaufman, Y. J.: Water vapour retrievals using Moderate Resolution Imaging Spectroradiometer (MODIS) near-infrared channels, J. Geophys. Res., 108, 4389, doi:10.1029/2002JD003023, 2003.

IPCC: Climate Change 2014: Impacts, Adaptation, and Vulnerability. Part A: Global and Sectoral Aspects. Contribution of Working Group II to the Fifth Assessment Report of the Intergovernmental Panel on Climate Change, edited by: C. B. Field, V. R. Barros, D. J. Dokken, K. J. Mach, M. D. Mastrandrea, T. E. Bili, M. Chatterjee, K. L. Ebi, Y. O. Estrada, R. C. Genova, B. Girma, E. S. Kissel, A. N. Levy, S. MacCracken, P. R. Mastrandrea, and L. L. White, Cambridge University Press, Cambridge, UK and New York, NY, USA., 2014.

Leblanc, T. and McDermid, I. S.: Accuracy of Raman lidar water vapour calibration and its applicability to long-term measurements., Appl. Optics, 47, 5592–603, 2008.

Liu, Z., Li, M., Zhong, W., and Wong, M. S.: An approach to evaluate the absolute accuracy of WVR water vapour measurements inferred from multiple water vapour techniques, J. Geodyn., 72, 86–94, doi:10.1016/j.jog.2013.09.002, 2013.

Mallet, M., Dulac, F., Formenti, P., Nabat, P., Sciare, J., Roberts, G., Pelon, J., Ancellet, G., Tanré, D., Parol, F., di Sarra, A., Alados, L., Arndt, J., Auriol, F., Blarel, L., Bourrianne, T., Brogniez, G., Chazette, P., Chevaillier, S., Claeys, M., D'Anna, B., Denjean, C., Der-

AMTD
8, 10577–10609, 2015

imian, Y., Desboeufs, K., Di Iorio, T., Doussin, J.-F., Durand, P., Féron, A., Freney, E., Gaimoz, C., Goloub, P., Gómez-Amo, J. L., Granados-Muñoz, M. J., Grand, N., Hamonou, E., Jankowiak, I., Jeannot, M., Léon, J.-F., Maillé, M., Mailler, S., Meloni, D., Menut, L., Momboisse, G., Nicolas, J., Podvin, J., Pont, V., Rea, G., Renard, J.-B., Roblou, L., Schepanski, K., Schwarzenboeck, A., Sellegri, K., Sicard, M., Solmon, F., Somot, S., Torres, B., Totems, J., Triquet, S., Verdier, N., Verwaerde, C., Wenger, J., and Zapf, P.: Overview of the Chemistry-Aerosol Mediterranean Experiment/Aerosol Direct Radiative Forcing on the Mediterranean Climate (ChArMEx/ADRIMED) summer 2013 campaign, Atmos. Chem. Phys. Discuss., 15, 19615–19727, doi:10.5194/acpd-15-19615-2015, 2015.

Pérez-Ramirez, D., Whiteman, D. N., Smirnov, A., Lyamani, H., Holben, B. N., Pinker, R., Andrade, M., and Alados-Arboledas, L.: Evaluation of AERONET precipitable water vapour vs. micro-wave radiometry, GPS, and radiosondes at ARM sites, J. Geophys. Res. Atmos., 119, 9596–9613, doi:10.1002/2014JD021730, 2014.

Randriamiarisoa, H., Chazette, P., Couvert, P., Sanak, J., and Mégie, G.: Relative humidity impact on aerosol parameters in a Paris suburban area, Atmos. Chem. Phys., 6, 1389–1407, doi:10.5194/acp-6-1389-2006, 2006.

Reiche, M., Funk, R., Zhang, Z., and Hoffmann, C.: Using a parafoil kite for measurement of variations in particulate matter – a kite-based dust profiling approach, Atmos. Clim. Sci., 2, 41–51, doi:10.4236/acs.2012.21006, 2012.

Schmid, B., Michalsky, J. J., Slater, D. W., Barnard, J. C., Halthore, R. N., Liljegren, J. C., Holben, B. N., Eck, T. F., Livingston, J. M., Russell, P. B., Ingold, T., and Slutsker, I.: Comparison of columnar water-vapour measurements from solar transmittance methods, Appl. Optics, 40, 1886, doi:10.1364/AO.40.001886, 2001.

Sherlock, V., Garnier, A., Hauchecorne, A., and Keckhut, P.: Implementation and validation of a Raman lidar measurement of middle and upper tropospheric water vapour, Appl. Optics, 38, 5838, doi:10.1364/AO.38.005838, 1999a.

Sherlock, V., Hauchecorne, A., and Lenoble, J.: Methodology for the independent calibration of Raman backscatter water-vapour lidar systems., Appl. Optics, 38, 5816–37, doi:10.1364/AO.38.005838, 1999b.

Turner, D. D., Whiteman, D. N., Evans, K. D., Melfi, S. H., Goldsmith, J. E. M., and Schwemmer, G. K.: Water vapour measurements by Raman lidar during the ARM 1997 Water Vapour Intensive Observation Period, in: IGARSS '98. Sensing and Managing the Environment,

AMTD
8, 10577–10609, 2015

1998 IEEE International Geoscience and Remote Sensing, Symposium Proceedings., vol. 4, 2155–2157, 1998.

Weckwerth, T. M., Wulfmeyer, V., Wakimoto, R. M., Hardesty, R. M., Wilson, J. W., and Banta, R. M.: NCAR–NOAA lower-tropospheric water vapour workshop, B. Am. Meteorol. Soc., 80, 2339–2357, doi:10.1175/1520-0477(1999)080<2339:NNLTWV>2.0.CO;2, 1999.

Weckwerth, T. M., Parsons, D. B., Koch, S. E., Moore, J. a., LeMone, M. a., Demoz, B. B., Flamant, C., Geerts, B., Wang, J., and Feltz, W. F.: An overview of the international H_2O project (IHOP_2002) and some preliminary highlights, B. Am. Meteorol. Soc., 85, 253–277, doi:10.1175/BAMS-85-2-253, 2004.

Whiteman, D. N., Melfi, S., and Ferrare, R.: Raman lidar system for the measurement of water vapour and aerosols in the Earth's atmosphere, Appl. Optics, 31, 3068–82, doi:10.1364/AO.31.003068, 1992.

Whiteman, D. N., Demoz, B., Schwemmer, G., Gentry, B., Di Girolamo, P., Sabatino, D., Comer, J., Veselovskii, I., Evans, K., Lin, R.-F., Wang, Z., Behrendt, A., Wulfmeyer, V., Browell, E., Ferrare, R., Ismail, S., and Wang, J.: Raman lidar measurements during the international H_2O project. Part I: Instrumentation and analysis techniques, J. Atmos. Ocean. Tech., 23, 157–169, doi:10.1175/JTECH1839.1, 2006a.

Whiteman, D. N., Demoz, B., Schwemmer, G., Gentry, B., Di Girolamo, P., Sabatino, D., Comer, J., Veselovskii, I., Evans, K., Lin, R.-F., Wang, Z., Behrendt, A., Wulfmeyer, V., Browell, E., Ferrare, R., Ismail, S., and Wang, J.: Raman lidar measurements during the international H_2O project. Part II: Case studies, J. Atmos. Ocean. Tech., 23, 170–183, doi:10.1175/JTECH1839.1, 2006b.

Whiteman, D. N., Venable, D., and Landulfo, E.: Comments on "Accuracy of Raman lidar water vapour calibration and its applicability to long-term measurements," Appl. Optics, 50, 2170–2176 (author reply 2177–2178), doi:10.1364/AO.50.002170, 2011.

Willitsford, A. and Philbrick, C. R.: Lidar description of the evapourative duct in ocean environments, in: Proc. SPIE Vol. 5885, Remote Sensing of the Coastal Oceanic Environment, edited by: R. J. Frouin, M. Babin, and S. Sathyendranath, 58850G, doi:10.1117/12.620948, 2005.

Wulfmeyer, V., Behrendt, A., Kottmeier, C., Corsmeier, U., Barthlott, C., Craig, G. C., Hagen, M., Althausen, D., Aoshima, F., Arpagaus, M., Bauer, H.-S., Bennett, L., Blyth, A., Brandau, C., Champollion, C., Crewell, S., Dick, G., Di Girolamo, P., Dorninger, M., Dufournet, Y., Eigenmann, R., Engelmann, R., Flamant, C., Foken, T., Gorgas, T., Grzeschik, M., Handw-

AMTD
8, 10577–10609, 2015

erker, J., Hauck, C., Höller, H., Junkermann, W., Kalthoff, N., Kiemle, C., Klink, S., König, M., Krauss, L., Long, C. N., Madonna, F., Mobbs, S., Neininger, B., Pal, S., Peters, G., Pigeon, G., Richard, E., Rotach, M. W., Russchenberg, H., Schwitalla, T., Smith, V., Steinacker, R., Trentmann, J., Turner, D. D., van Baelen, J., Vogt, S., Volkert, H., Weckwerth, T., Wernli, H., Wieser, A., and Wirth, M.: The convective and orographically-induced precipitation study (COPS): the scientific strategy, the field phase, and research highlights, Q. J. Roy. Meteor. Soc., 137, 3–30, doi:10.1002/qj.752, 2011.

AMTD
8, 10577–10609, 2015

Table 1. Characteristics of the WVMR in-situ sounding apparatus.

Balloon rawinsounding (CNES), Modem GPSonde M10 (150g)	
Altitude range	100 m–36 km a.m.s.l.
Measurements	Temperature, RH, GPS altitude
Meas. period	1 s
Temp. uncertainty	±0.5 °C
RH uncertainty	±5 %
Altitude uncertainty	±10 m (±1 hPa down to 0.4 hPa at 10 km a.m.s.l.)
→ WVMR error	±1.2 g kg^{-1} down to ±0.04 g kg^{-1} at 10 km a.m.s.l.
Kite PTU sonde (LSCE), Vaisala modules & recorder (360g)	
Altitude range	5–400 m
Measurements	Temperature, RH, Pressure
Meas. period	10 s
Temp. uncertainty	±0.15 °C
RH uncertainty	±2 %
Pressure uncertainty	±0.6 hPa
→ WVMR error	±0.6 g kg^{-1} (below 500 m)

AMTD
8, 10577–10609, 2015

Table 2. Statistics for the comparison between various integrated water vapour content retrievals and the lidar (simultaneous measurements within ±1 h).

	Mean bias (cm)	SD (cm)	Mean Rel. Bias (%)	Rel. SD (%)
Sunphotometer	−0.93	0.92	−28	28
ECMWF	−0.08	0.26	−1.5	8.9
ECMWF (w/o 6/14)	−0.12	0.18	−2.7	5.8
MODIS	−0.17	0.50	−3.1	15.6
Radiosoundings	−0.15	0.19	−4.0	6

AMTD
8, 10577–10609, 2015

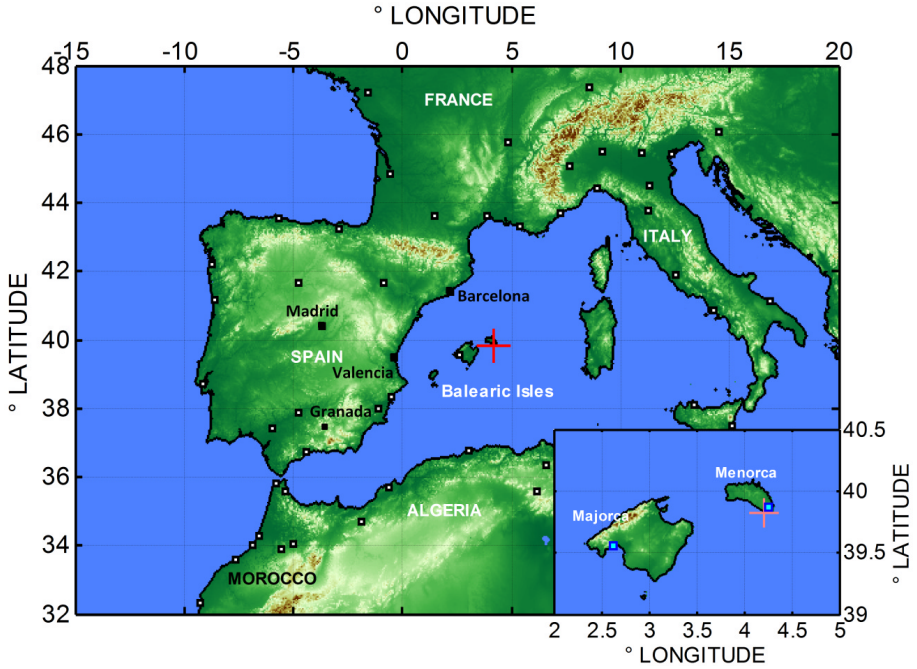

Figure 1. Situation map of the Menorca/Cap d'en Font station (red cross). The location of radiosoundings on Menorca and Majorca Islands is shown as blue squares within the insert.

AMTD
8, 10577–10609, 2015

Figure 2. View of the kite and lightweight PTU probe used for lidar calibration.

AMTD
8, 10577–10609, 2015

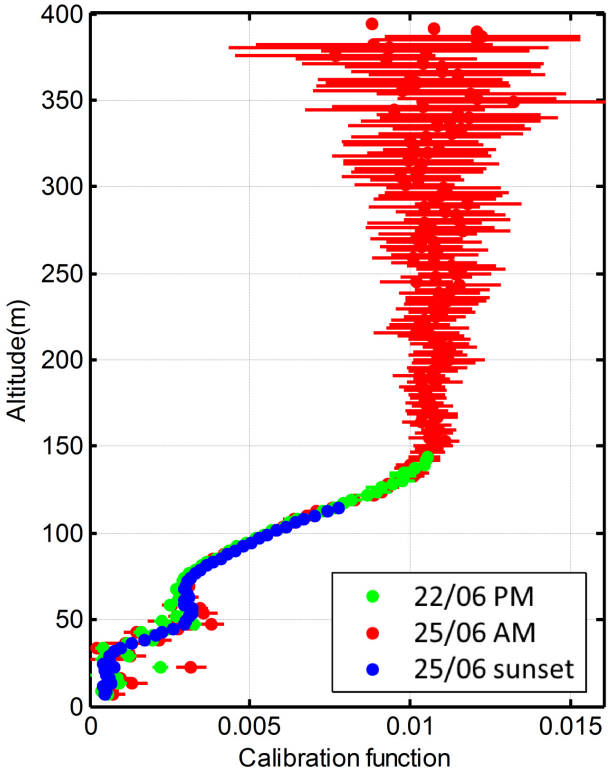

Figure 3. Results of lidar calibration by kite-carried PTU, in terms of calibration function $C(z) = \xi_{H_2O}(z)/K_{WVMR}$ (dots) as measured during 3 separate flights: on 22 June afternoon up to 140 m, on 25 June morning up to 390 m, on 25 June at sunset up to 115 m, the latter providing less noisy estimations of the overlap function at low altitude. RMS error combining lidar signal noise and sounding errors is shown as horizontal bars. The assessed calibration constant is $94.8 \pm 2.0\,g\,kg^{-1}$ (mean over the 3 flights).

AMTD
8, 10577–10609, 2015

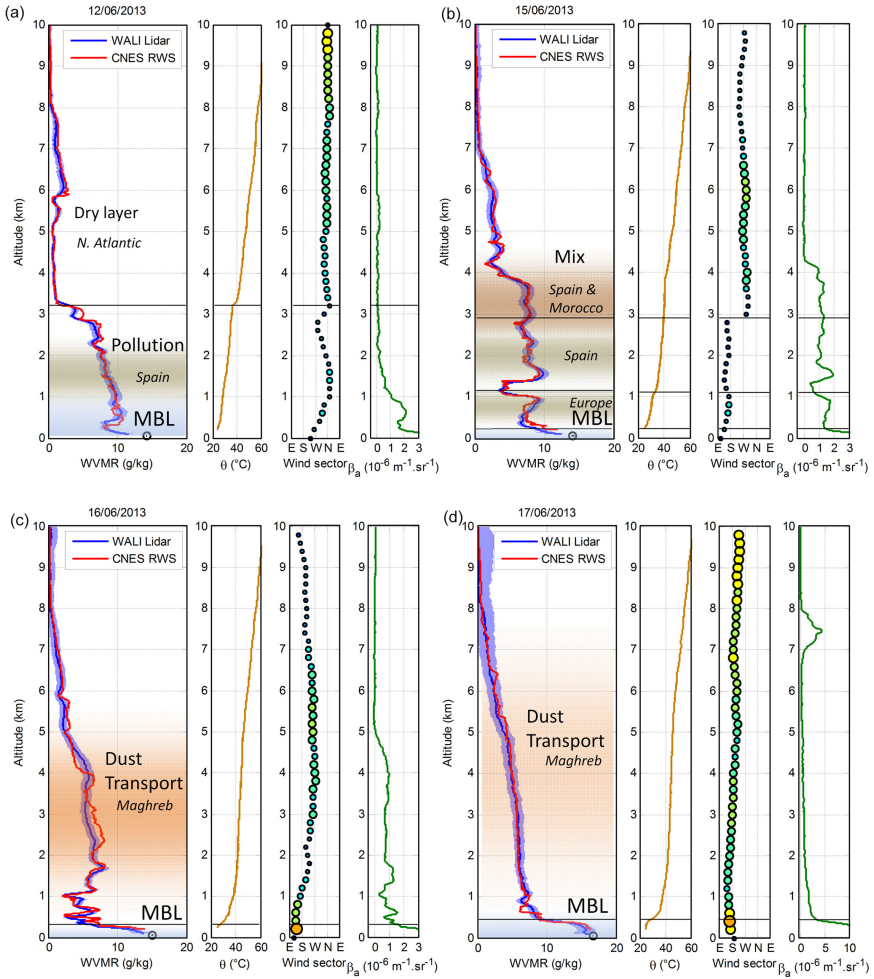

AMTD
8, 10577–10609, 2015

Relevance of a kite-based calibration for a water vapour Raman lidar

J. Totems and P. Chazette

Figure 4. Comparison of lidar WVMR measurements to 4 rawinsoundings performed from Sant-Lluis air field on the evenings of **(a)** 12 June, **(b)** 15 June, **(c)** 16 June and **(d)** 17 June 2013 (approximately 21:00–23:00 LT), under varied aerosol loads and atmospheric water contents. The red line is the radiosonde-derived WVMR and the blue line is the one obtained by lidar, with its standard deviation represented as a blue-shaded area. The black circle at zero altitude indicates WVMR as measured on the ground. Potential temperature θ, wind sector and velocity (shown as circle size and colour, measured by the radiosonde), as well as aerosol backscatter coefficient profiles (measured by the lidar) are also given for reference. Layer boundaries as indicated by wind shears and strong potential temperature gradients are denoted by black lines. Origins and contents of air masses as deduced by backtrajectories (HYSPLIT, Draxler and Rolph, 2015) are given in plain text. The lidar integration time is equal to the balloon ascent, i.e. approximately 40 min. MBL = Marine Boundary Layer.

AMTD
8, 10577–10609, 2015

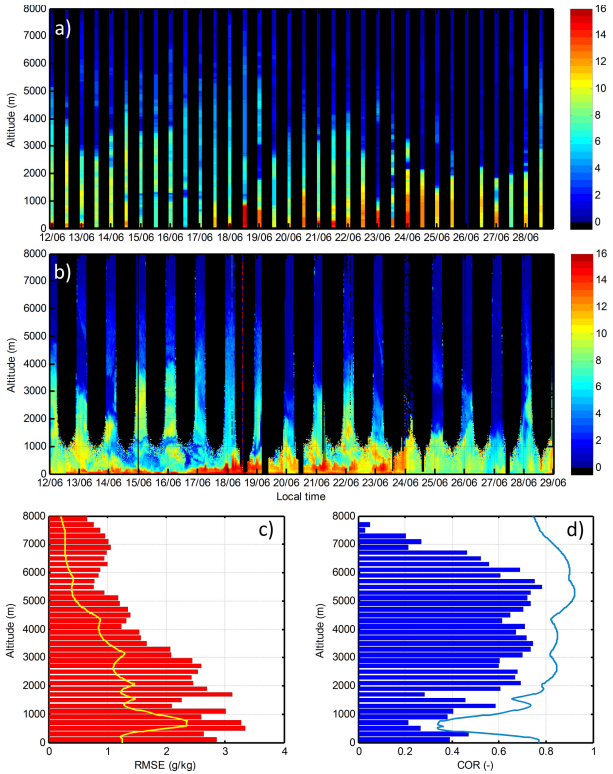

Figure 5. (a) WVMR derived from operational radiosoundings at Palma de Majorca (~ 135 km E–SE of Cap d'en Font), for 16 days of June 2013, **(b)** lidar WVMR for the same period, **(c)** root mean square error and **(d)** correlation between coincident profiles as a function of altitude (RMSE and COR as defined in Boylan and Russell, 2006); bars are measurements, whereas continuous coloured lines show the natural variability as evaluated on the ECMWF/IFS fields between the two locations.

AMTD
8, 10577–10609, 2015

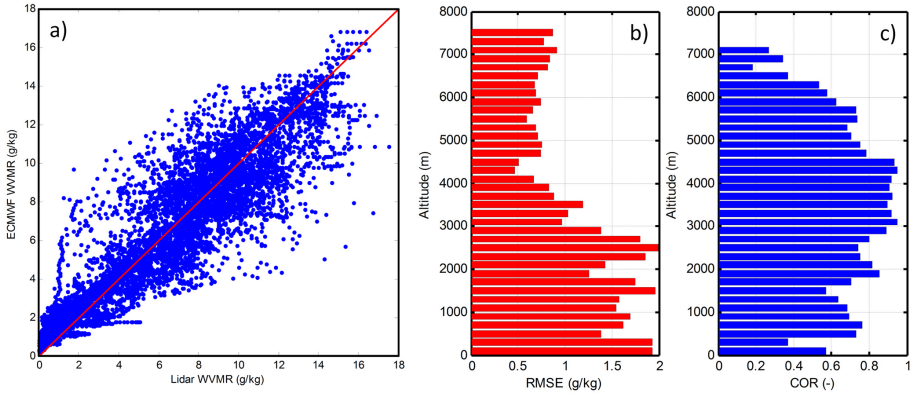

Figure 6. (a) Scatter plot between ECMWF and lidar-derived WVMR over all simultaneous measurements (blue dots). The red line is the identity. **(b)** RMS deviations and **(c)** correlation between coincident profiles as a function of altitude.

AMTD
8, 10577–10609, 2015

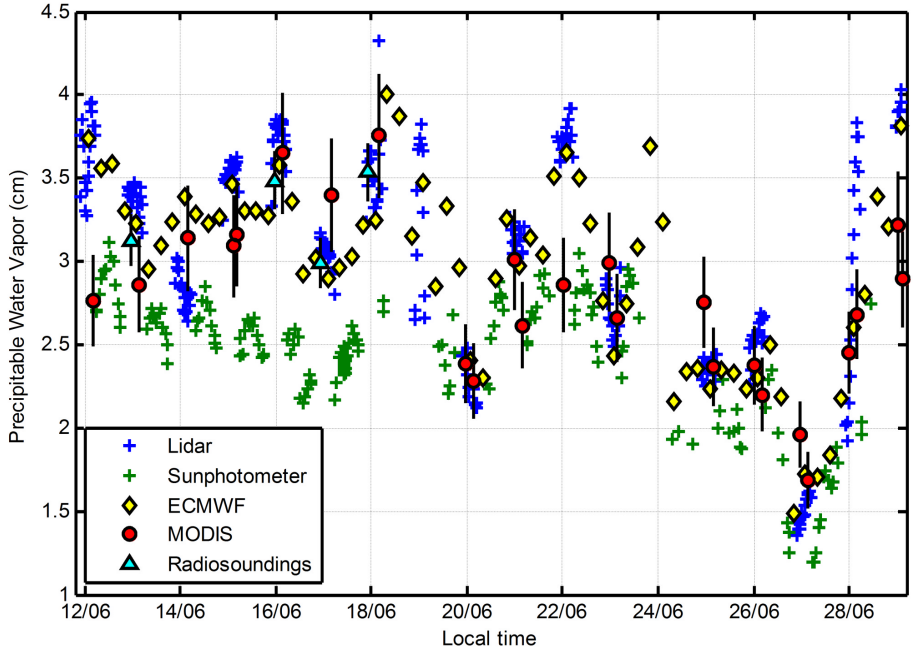

Figure 7. Comparison of various retrievals of integrated water vapour content (precipitable water vapour, PWV, in cm) from 12 to 19 June 2013: by lidar (blue), MODIS (average within a 10 km radius area around the lidar, discarding cloudy pixels with lower PWV, green circles), adding ECMWF 0.5° model reanalyses (interpolation, yellow diamonds) and radiosoundings at Menorca (cyan triangles, error bars computed after uncertainty in Table 1) as a reference. Error bars given for MODIS represent 10 % relative error (Pérez-Ramirez et al., 2014).

AMTD
8, 10577–10609, 2015